Reduced repertoire of cortical microstates and neuronal ensembles in medically induced loss of consciousness

Michael Wenzel, Shuting Han, Elliot H. Smith, Erik Hoel, Bradley Greger, Paul A. House, Rafael Yuste

SUPPLEMENTAL INFORMATION

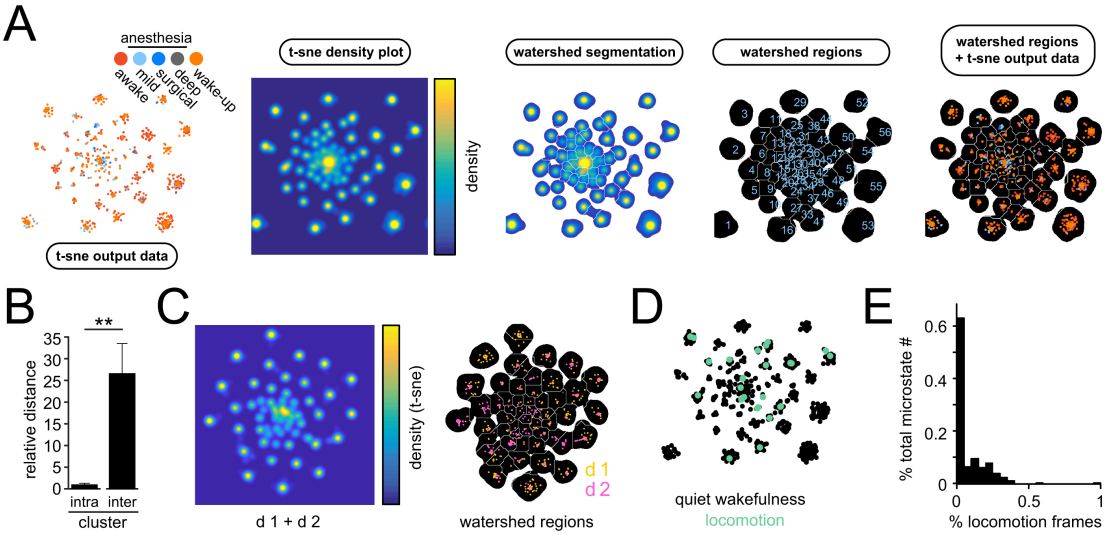

Suppl. Figure 1 T-SNE/watershed segmentation of neural activity – microstate stability – state occurrence across quiet wakefulness and locomotion
Refers to Fig. 1 and 2.
A) T-SNE and watershed segmentation of neural activity in mice. From left to right: 2-dimensional embedding space obtained by t-SNE, datapoints (=frames) from different conditions are individually colored. A density plot is created and clusters of similar activity are separated by watershed segmentation. Thereupon, the number of discriminable watershed regions (=microstates) can be identified, and it can be analyzed how specific frames from individual conditions contribute to each microstate. **B)** Avg distances between members of an identified watershed region (intra) were compared to avg distances between regions (inter) to insure robust cluster identification within the embedding space. Distances between members of a region were consistently significantly smaller than distances between regions (n=7mice; total # of watershed regions= 425 [60.7 ± 9 s.e.m.], total number of active frames = 34321 [4903 ± 929 s.e.m.], student's t-test p=0.0081). **C)** Microstates are stable across days. Representative exp. of 2 imaging sessions of the same neural network (visual cortex, layer 2/3, 62 neurons) separated by 24hrs. Left: t-sne density space of the 2 sessions. Right: WS analysis of the t-SNE space identified a total of 55 microstates. 55 were present on exp. day 1 (orange), 54 on exp. day 2 (magenta). **D)** Locomotion triggers microstates that are present during quiet wakefulness. Paradigmatic t-SNE space from the exp. shown in Fig. 1 E-G prior to WS. Each black dot corresponds to a frame containing neural activity. Frames during locomotion are highlighted in green. Note how all motion frames project onto existing conglomerates of non-locomotion frames. **E)** Quantification of locomotion-triggered microstates. Histogram containing all 425 microstates across 7 mice derived from t-SNE/WS (y-axis, in %) vs. the % of locomotion frames contributing to a respective cluster (x-axis). Most microstates (99.53%) comprised predominantly non-motion frames. One microstate (0.24%) exclusively contained locomotion frames. One additional microstate (0.24%) contained predominantly locomotion frames (57%).

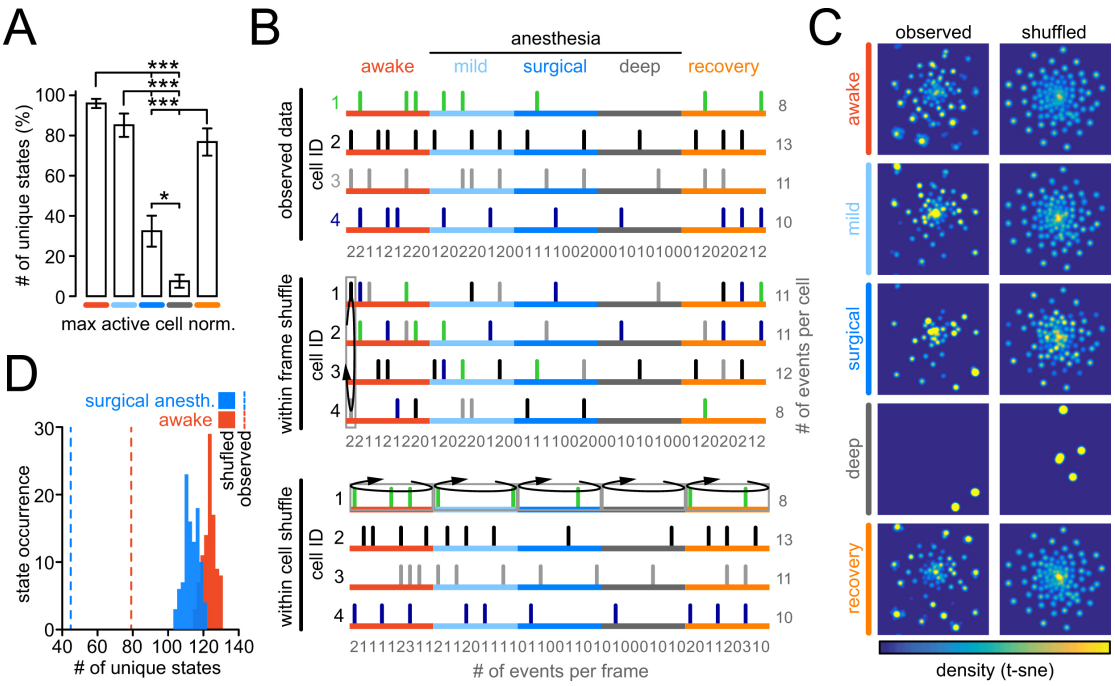

Suppl. Figure 2 Dependence of microstate number on neural coactivity – Re-shuffling approaches
Refers to Fig. 1 and 2.
A) Number of unique microstates across conditions as % of all identified unique microstates in a given exp., across animals (n=7 mice). The difference to Figure 1 K is that here the max. number of coactive cells allowed per condition was determined by the max. number of cells being observed during surgical anesthesia (n=7mice, # of max. coactive cells during surgical anesthesia = 2.6 ± 0.4 s.e.m.). All frames surpassing this maximum were dismissed from the analysis. This was done to account for a potentially unfair advantage of milder anesthetic conditions or wakefulness over surgical anesthesia based on coactivity patterns that could not occur during surgical anesthesia. However, even when handled this way, the resulting analysis was consistent with the one displayed in Figure 1 K.1-way anova with Bonferroni post-hoc test (n=7 mice, 5 conditions [df=4], *p<0.05, **p<0.01, ***p<0.001). **B)** Re-shuffling approaches illustrated on the activity of four example neurons. Upper panel: The input matrix represents an observed raster plot of neural firing across anesthetic conditions (5 conditions, 9 frames each). Gray numbers underneath the plot show summed-up within-frame activity for each frame displayed. Gray numbers on the right represent summed-up activity for each neuron displayed. Middle panel: 'within frame' shuffling randomly permutates, frame by frame firing within every frame (black arrow), that is, overall network activity is kept constant with regards to the observed data (numbers underneath each frame are the same es in observed), while within frame patterns are randomized (gray numbers to the right of each neuron change as compared to observed data). Lower panel: raster plot shown in upper panel serves as the input matrix, again. To randomize coactivity patterns in each anesthetic condition, firing is randomized 'within cell'. For each condition separately, firing within each neuron is randomized across time (black arrows). The result is a maintained overall firing per neuron (gray numbers to the right of neurons are identical to those in the observed data), while within frame coactivity is randomized (gray numbers underneath frames differ from observed data). **C)** Same exp. as shown in Fig. 1G. Comparative visualization of embedding spaces obtained from observed data (upper panel) and 1 of the 100 corresponding randomized datasets (lower panel, obtained by within-frame shuffling). Note that consistently across conditions, corresponding randomized data produced visibly more watershed regions, spread out evenly across the embedding space as opposed to the observed data. Note also how even during surgical anesthesia, despite reduced overall activity, a large number of microstates is theoretically possible (see also D, and Fig. 1L). **D)** Representative exp.: total number of observed unique microstates (dashed lines) during wakefulness (red) or surgical anesth. (blue) vs. corresponding distributions of values from 100 randomized datasets. No overlap of observed vs. random data (p<0.01, see also Fig. 1L).

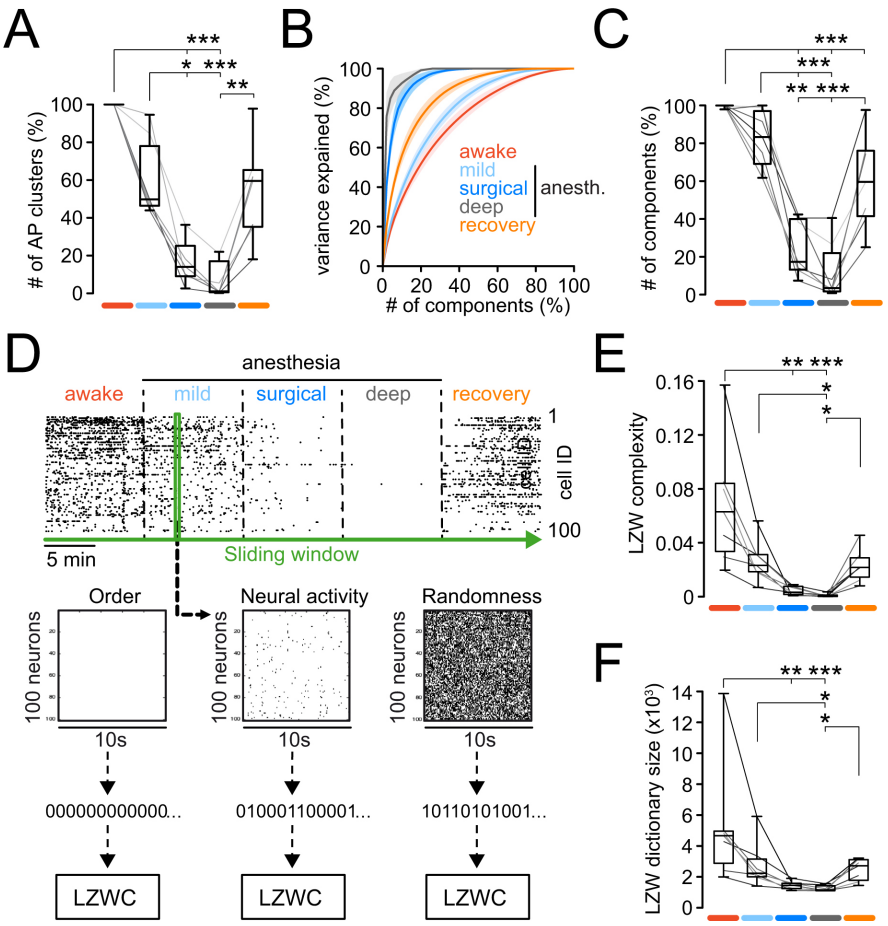

Suppl. Fig. 3. Alternative analytical approaches (APC, LZWC, PCA) – Microstate number per fixed activity Refers to Fig. 1 and 2.

A) Boxplots of number of unique microstates (APC, see methods) across conditions as % of all identified unique microstates in a given exp.; line plots are individual exp. (grayscale) **B)** Cumulative percentage of the variance explained for each experimental condition across exp.. Number of PCA components (see methods) normalized (%) for comparison across exp.. Solid lines represent the respective mean value, shaded areas represent s.e.m.. **C)** Boxplots of number of PCA components across conditions as % of all identified components in a given experiment; line plots are individual experiments (grayscale). **D)** Measuring Lempel-Ziv-Welch complexity (LZWC) of local neural activity. Top panel: Same raster plot of neural firing of 100 neurons imaged across five experimental conditions (10min each) as shown in fig. 1F. A sliding window (green) is moved across the matrix to calculate LZWC. Middle panel: Two windows of identical size to the sample window of neural activity are generated, one of perfect order (all zeroes or all ones) and one of complete randomness (random number generator). Bottom panel: Each window is transformed into a string of ones and zeroes, and the LZW algorithm is used to compress each string. The final length of the compressed string, compared to its original length, determines its compressibility (see methods). **E)** Boxplots of LZW complexity across conditions; line plots are individual exp. (grayscale). **F)** Boxplots of LZW dictionary size across conditions; line plots are individual exp. (grayscale).

All boxes in boxplots represent 25-75%ile of the data, bars within boxes represent means. Statistical analyses in A, C, E, and F represent 1way-anova with Bonferroni post-test. *p<0.05, **p<0.01, ***p<0.001.

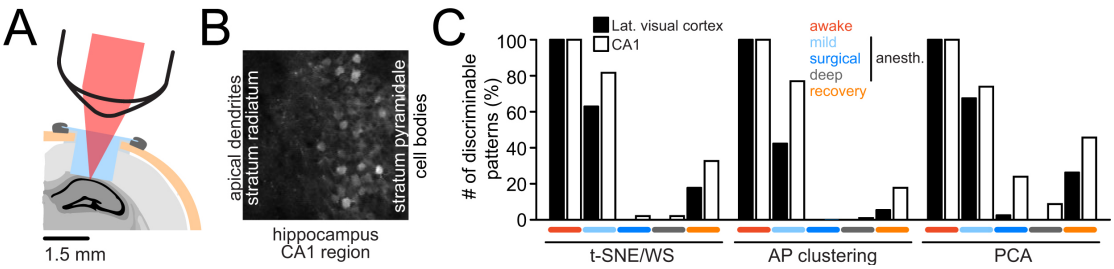

Suppl. Fig. 4. Microstate reduction during mLOC in mice is found across sensory and higher order cortex
Refers to Fig. 1 and 2

A) Sketch of experimental setup for hippocampal imaging. A small area of cortex (~1.5x1.5mm, neocortex in light gray) above left CA1 is removed, and replaced with a UV-sterilized glass plug (1.5x1.5mm) attached to a thin glass coverslip (both in light blue). The plug is fixed in place with a slim meniscus of silicon around the edge of the glass cover and by applying small amounts of dental cement (dark gray) around the edge of the glass cover resting on the skull (yellow). After a recovery period of at least 2 weeks, hippocampal two-photon imaging is performed during mLOC (please see methods). **B)** Two-photon avg image of field of view showing hippocampal CA1 cell bodies in stratum pyramidale (right) and CA1 apical dendrites in stratum radiatum (left). **C**) Number of discriminable patterns (in % of identified patterns during wakefulness) across mLOC in experiments in lateral visual cortex (layer 2/3, 104 neurons, black bars) or hippocampal CA1 (stratum pyramidale, 80 neurons, outlined bars) identified either by t-SNE/Watershed segmentation (left), AP clustering (middle), or PCA component analysis (right). Consistent with our experiments in primary sensory cortex in mice, the number of discriminable patterns of activity decreases strongly with increasing anesthetic depth across analytical approaches, and recovers during the wakeup period.

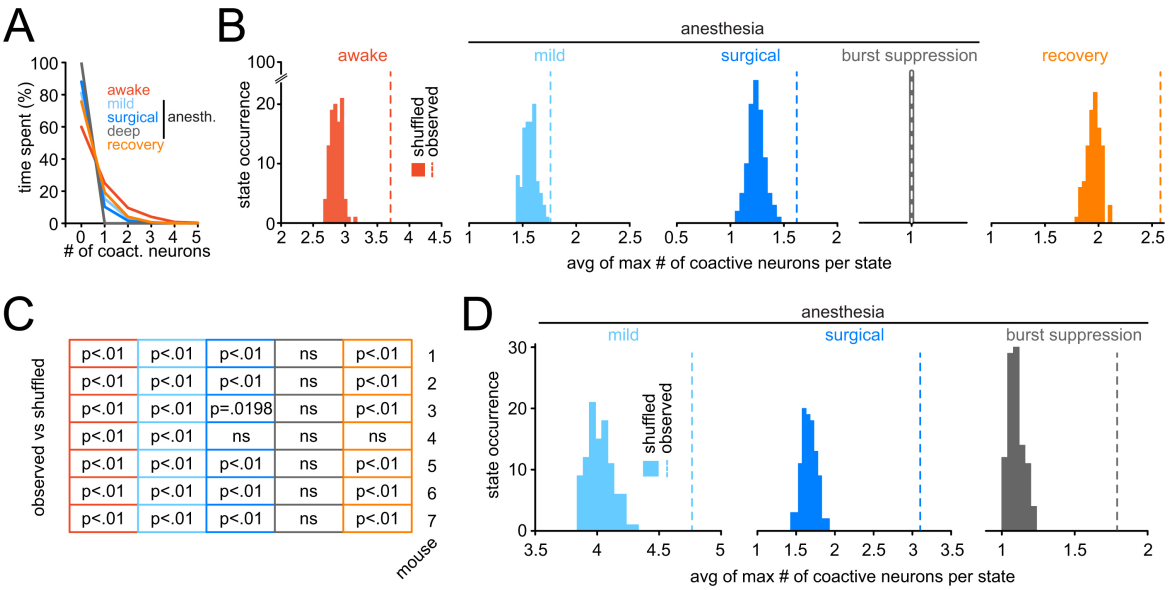

Suppl. Fig. 5. Observed coactivity patterns in mice and humans are non-random – ensemble fragmentation upon mLOC

Refers to Fig. 1 M-N (mice), and Fig. 2 M-N (humans).

A) Representative exp.: Number of co-active neurons versus the time spent by population in frames containing such co-activity, displayed per condition. Please see also Fig. 1 M. **B)** Representative experiment. Displayed for each experimental condition is the observed average of the maximum number of coactive cells participating in each detected discriminable microstate (dotted line) versus 100 values derived from 100 within-cell-shuffled randomized datasets (colored distributions). Randomized values consistently showed less coactivity than the observed data, with no overlap between the shuffled distributions and the observed values ($p<0.01$). This showed that the observed coactivity patterns were non-random, and that significanlty higher coactivity patterns could be found in the observed data than expected by chance. **C)** p values for the process shown in B), for all 7 experiments in mice. A p value <0.05 corresponds to the observed value being bigger/smaller than 95% of the 100 values obtained from randomized datasets; $p<0.01$ corresponds to the observed value being smaller/bigger than all 100 values obtained from randomized datasets; ns=not significant. Ns in all burst suppression conditions could be explained by a critically low overall activity (Fig. 1I). **D)** Same as in B), yet in one of the two human subjects, across three anesthetic depths ($p<0.01$ in all conditions; for the second patient: $p<0.01$ for mild and surgical anesthesia, ns for burst suppression anesthesia). The results are consistent with those observed in mice.